

PAPER • OPEN ACCESS

## Exploring the limits to quantitative elastography: supersonic shear imaging in stretched soft strips

To cite this article: Samuel Croquette *et al* 2025 *Phys. Med. Biol.* **70** 145009

View the [article online](#) for updates and enhancements.

You may also like

- [A hybrid predictor-corrector network and spatiotemporal classifier method for noisy plant PET image classification](#)  
Weike Chang, Nicola D'Ascenzo, Emanuele Antonecchia *et al.*
- [Limited-angle SPECT image reconstruction using deep image prior](#)  
Kensuke Hori, Fumio Hashimoto, Kazuya Koyama *et al.*
- [Quantification of the tumour microvascular response to high dose-per-fraction radiotherapy](#)  
W Jeffrey Zabel, Hector A Contreras-Sanchez, Nader Allam *et al.*

## Empowering Automation. Driving Efficiency.

- Learn to code for your clinic through Gateway Scripts Clinical Schools.

**Start Your Journey  
Now**





## PAPER

## OPEN ACCESS

RECEIVED  
13 March 2025REVISED  
24 June 2025ACCEPTED FOR PUBLICATION  
30 June 2025PUBLISHED  
11 July 2025

Original Content from  
this work may be used  
under the terms of the  
[Creative Commons  
Attribution 4.0 licence](#).

Any further distribution  
of this work must  
maintain attribution to  
the author(s) and the title  
of the work, journal  
citation and DOI.



# Exploring the limits to quantitative elastography: supersonic shear imaging in stretched soft strips

Samuel Croquette , Alexandre Delory , Daniel A Kiefer , Claire Prada and Fabrice Lemoult\*

Institut Langevin, ESPCI Paris, Université PSL, CNRS, 75005 Paris, France

\* Author to whom any correspondence should be addressed.

E-mail: [fabrice.lemoult@espci.psl.eu](mailto:fabrice.lemoult@espci.psl.eu)**Keywords:** elastography, supersonic shear wave imaging, guided elastic waves, viscoelasticity, acoustoelastic effect

## Abstract

**Objective.** Shear wave elastography has enriched ultrasound medical imaging with quantitative tissue stiffness measurements. We aim to explore the limitations that persist related to viscoelasticity, guiding geometry or static deformation. **Approach.** A nearly-incompressible soft elastomer strip is chosen to mimic the mechanical behaviour of an elongated tissue. A supersonic shear wave scanner measures the propagation of shear waves within the strip. It provides a wide range of shear wave velocities, from 2 to 6 m s<sup>-1</sup>, depending on the frequency, the static strain as well as the orientation of the strip. **Main results.** To explain these different measurements, the guided wave effect is highlighted and analysed from the dispersion diagrams provided by the spatio-temporal Fourier transform of the raw data. The guided waves are then described using a material model that accounts for both the rheology and the hyperelastic behaviour, and allows to extract the mechanical parameters of the sample. **Significance.** To overcome some limitations of current elastography, we propose a theoretical framework which allows the simultaneous characterization of the viscoelastic and hyperelastic properties of soft tissues, paving the way for robust quantitative elastography of elongated tissues.

## 1. Introduction

Elastography, a non-invasive medical imaging technique, offers insights into tissue elasticity akin to traditional palpation but with greater precision. By quantifying tissue deformation in response to external mechanical forces such as compression or shear waves, elastography provides information on valuable mechanical properties. This technique has proven particularly useful in diagnosing conditions like liver fibrosis (Sandrin *et al* 2003, Asbach *et al* 2010, Deffieux *et al* 2015, Kennedy *et al* 2018), breast lesions (Sinkus *et al* 2005, Barr and Zhang 2012, Barr 2019), prostate cancer (Correas *et al* 2013), thyroid nodules (Cantisani *et al* 2015), heart problems (Elgeti and Sack 2014, Sinkus 2014, Hansen *et al* 2015, Khan *et al* 2018, Pruijssen *et al* 2020), tendinopathies (Farron *et al* 2009, Prado-Costa *et al* 2018, Mifsud *et al* 2023) and other musculoskeletal disorders (Paluch *et al* 2016, Winn *et al* 2016, Taljanovic *et al* 2017, Davis *et al* 2019).

Utilizing ultrasound imaging, magnetic resonance imaging, or optical coherence tomography, elastography records tissue displacement dynamics for stiffness assessment (Ormachea and Parker 2020). While various methodologies exist across imaging modalities for stiffness evaluation, recent years have seen significant advancements in optical coherence elastography (OCE) (Zvietcovich and Kirill 2022, Leartprapun and Adie 2023), particularly in ophthalmology (Kirby *et al* 2017, Lan *et al* 2023), but also in magnetic resonance elastography (MRE) (Low *et al* 2016, Sack 2023) with clinical applications involving large tissue regions like the breast (Sinkus *et al* 2005), heart (Elgeti and Sack 2014, Khan *et al* 2018, Marlevi *et al* 2020) and brain (Hiscox *et al* 2016).

Ultrasound, the most widely used elastography method (Shiina 2014, Sigrist *et al* 2017), offers real-time and in-depth tissue elasticity assessment, notably through acoustic radiation force methods (Doherty *et al* 2013). In this study, we employ supersonic shear wave imaging (SSI) (Bercoff *et al* 2004, Deffieux 2008) with

an Aixplorer™ system, measuring the shear wave velocity  $V_T$  to deduce the shear modulus  $\mu$  and the Young's modulus of the tissue. Indeed, in an incompressible material of mass density  $\rho$ , they are calculated from this velocity using the simple relation  $E = 3\mu = 3\rho V_T^2$ .

However, this equation only holds under certain strong assumptions that are rarely valid, thus limiting the robustness of quantitative elastography. These limitations can be attributed to four different causes. First, the viscoelasticity of a tissue leads to frequency-dependent mechanical parameters, including the deduced Young's modulus (Kennedy *et al* 2014, 2018, Sinkus 2014, Hiscox *et al* 2016, Low *et al* 2016, Kirby *et al* 2017). Second, tissues like muscles are inherently anisotropic and  $V_T$  strongly depends on the propagation direction of the wave (Sinkus 2014, Prado-Costa *et al* 2018, Mifsud *et al* 2023). Third, most tissues have boundaries and act as waveguides, leading to strong dispersion (Kirby *et al* 2017, Li *et al* 2017, Khan *et al* 2018, Pelivanov *et al* 2019, Ramier *et al* 2019). Last, surrounding fluids or other external factors may apply a prestress in the tissue of interest, leading again to changes in the measured velocity (Elgeti and Sack 2014, Cantisani *et al* 2015, Hansen *et al* 2015, Li *et al* 2017, Barr 2019) due to acoustoelasticity. It is common that biological tissues combine several of the above-mentioned aspects as it is highlighted in several reviews involving different imaging modalities (Sigrist *et al* 2017, Bilston 2018, Davis *et al* 2019, Ormachea and Parker 2020, Caenen *et al* 2022, Crutison *et al* 2022, Zvietcovich and Kirill 2022, Lan *et al* 2023, Leartprapun and Adie 2023). These limits are known and still the subject of active research.

We have developed a strong expertise in modelling elastic waves in soft waveguides, notably on the combined roles of viscoelasticity and acoustoelasticity (Lanoy *et al* 2020, Delory *et al* 2022, 2024). Recently, the dispersion curves in a stretched free strip (Delory *et al* 2024) have been studied and accurate predictions have been made. In this context, we believe it is straightforward to compare conventional elastography measurements with results obtained using the model developed within the frameworks of visco-acoustoelasticity.

In this article, using a simple silicone strip immersed in water and a standard ultrasound sequence, we provide tools to overcome the issues raised by the combination of viscoelasticity, waveguiding geometry and prestress. The anisotropy is also naturally considered since prestress leads to extrinsic anisotropy for the propagation of shear waves in soft media (Delory *et al* 2023). By applying large deformations to the viscoelastic strip in different orientations, a wide range of phase velocities is measured. First, we identify the nature of the generated shear waves. Then, combining our previous works (Delory *et al* 2023, 2024) with the method described in Kiefer *et al* (2019), we predict their dispersion curves and phase velocities. Finally, we are able to capture the frequency and elongation-dependent nature of the mechanic properties of the material.

## 2. Methods

We first describe the experiment and rheology. After a few finite elements simulations, we then introduce the new elasticity tensor that accounts for visco-elasticity and hyper-elasticity. We finally comment its numerical implementation for guided waves.

### 2.1. Rheological characterization of Ecoflex-OO20

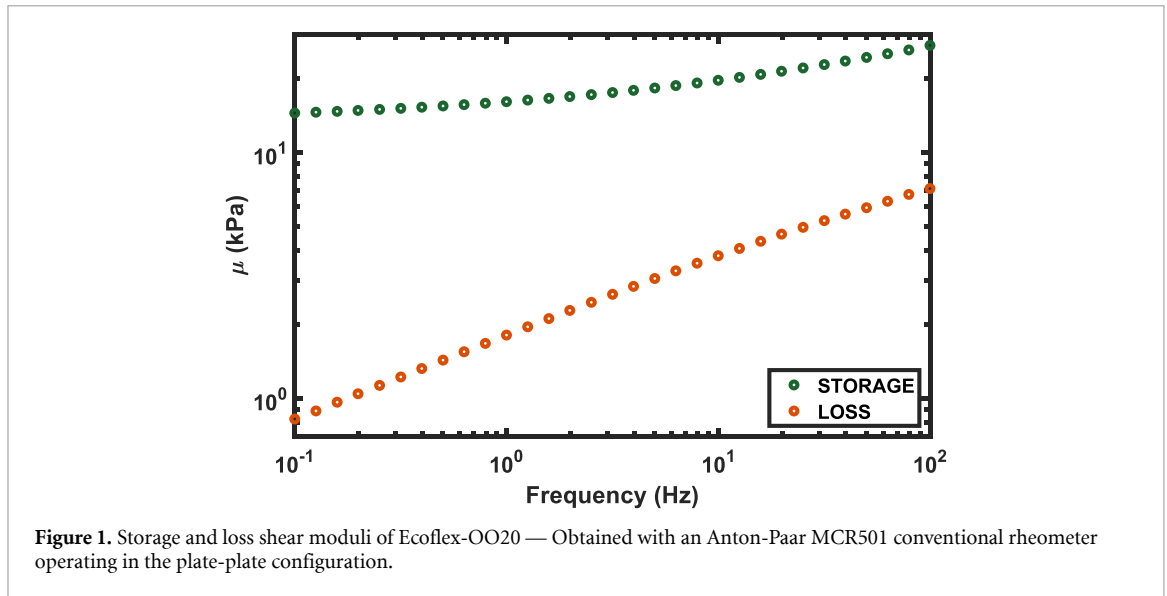
The soft material investigated throughout this article is Smooth-On Ecoflex-OO20. This material, selected for its similarity to biological tissues and its practical advantages over agar gels (e.g. stability over time), is prepared by mixing equal quantities of a polymer and its crosslinking agents. While the properties of Ecoflex are well-documented in the literature (Liu *et al* 2014, Kearney *et al* 2015, Brinker and Klatt 2016, Liao *et al* 2021, Delory *et al* 2022), we conducted rheological measurements on our samples to reduce uncertainties.

A conventional rheometer (Anton-Paar MCR501) operating in the plate-plate configuration was used to examine the rheology. A sample was cured directly in the rheometer. Both the real (storage modulus) and imaginary (loss modulus) parts of the shear modulus measured for frequencies ranging from 0.1 to 100 Hz are depicted in figure 1.

In such a logarithmic scale, the loss modulus appears to vary linearly while the storage modulus slowly increases after a particular frequency, as already observed in the literature for other elastomers of the Ecoflex range (Henni *et al* 2011). As the slope of the loss modulus is not an integer, here almost 1/3, a fractional derivative model needs to be used. One of the simplest models which satisfies the Kramers–Kronig relations is the fractional derivative Kelvin–Voigt model (Smit and De Vries 1970, Bagley and Torvik 1983, Liu *et al* 2014, Rolley *et al* 2019, Mainardi 2022, Sharma *et al* 2023), where the shear modulus takes the form:

$$\mu(\omega) = \mu_0 [1 + (i\omega\tau)^n] \quad (1)$$

where  $\omega$  is the angular frequency and  $\mu_0$ ,  $\tau$ ,  $n$  are parameters of the model. This viscoelastic model has become widespread in soft mechanics literature (Sharma *et al* 2023) and is recommended to describe the



behavior of soft tissues (Parker *et al* 2019) as well as the Ecoflex silicone considered here (Yasar *et al* 2013, Liu *et al* 2014).

The rheological measurements are fitted using this model. The best parameters to describe the experimental data points were found equal to:  $\mu_0 = 12$  kPa,  $\tau = 3.7$  ms, and  $n = 0.30$ .

## 2.2. Conventional shear wave elastography of a strip made of Ecoflex-OO20

A strip is placed in a water tank and acts as a waveguide for shear elastic waves. It is made of the aforementioned elastomer, Ecoflex-OO20, and prepared with a thickness of  $h = 2.7$  mm, a width of  $b = 4$  cm, and a length of  $L_0 = 20$  cm. Elastography experiments are performed using an Aixplorer<sup>TM</sup> ultrasound system and a curved array XC6-1 transducer from Supersonic Imaging. This array offers a large field of view, and up to 14 cm of the strip is visible in the B-mode of the scanner when the strip is positioned at a depth of 6 cm. A default SSI ultrasound sequence is used, consisting of 5 push lines, each composed of 4 push depths. After each push line, the transducer switches to imaging mode (framerate of 1750 frames per second) to follow, in real-time, the generated shear waves (Bercoff *et al* 2004, Deffieux 2008).

As described in figure 2, two orientations of the strip are studied. In both of them, the transducer array is parallel to the strip axis  $x_1$ , and each push line generates a displacement along  $x_3$ . In the plate orientation depicted in figure 2(a), the imaging plane cuts the strip along its thickness and an out-of-plane displacement is generated. Conversely, in the strip orientation shown in figure 2(b), the imaging plane cuts the strip along its width and an in-plane displacement is generated in the strip. For both orientations, the scanner evaluates the velocity of the waves within the strip using its own commercially used procedure.

To observe the acousto-elastic effect, elongations are applied to the strip along the  $x_1$  axis. This is achieved by clamping the two ends of the strip in a rigid aluminium frame and adjusting the distances between the two edges of this frame. The shear wave measurements are then repeated for various elongations, quantified by the stretch ratio  $\lambda_1$  (elongated length divided by undeformed length), and for both orientations.

## 2.3. Finite element simulations of guided elastic waves in a strip immersed in water

To obtain the dispersion relations of waves guided by an elastic strip immersed in water, we utilize finite element simulations (specifically COMSOL Multiphysics 5.5). We consider a strip of thickness  $h = 2.7$  mm, width  $b = 4$  cm, length  $a = 1$  mm and density  $1.07$  g cm<sup>-3</sup>, with a longitudinal velocity of  $1000$  m s<sup>-1</sup> (Delory *et al* 2022) and transverse velocity of  $5.31$  m s<sup>-1</sup>. A Bloch periodic boundary condition is applied along the length for a discrete set of wavenumbers  $k$ . For each value, an eigenproblem is solved to obtain the four lowest eigenfrequencies as well as the corresponding eigenfields. To reduce computation time, only one fourth of the strip is simulated by applying different symmetry constraints with respect to the width and thickness middle planes. In this simulation, the motion of the strip induces displacements of the surrounding water. Perfectly matched layers are used to mimic a non-reflecting infinite water domain. The relevant dispersion curves corresponding to both orientations are presented in figure 3.

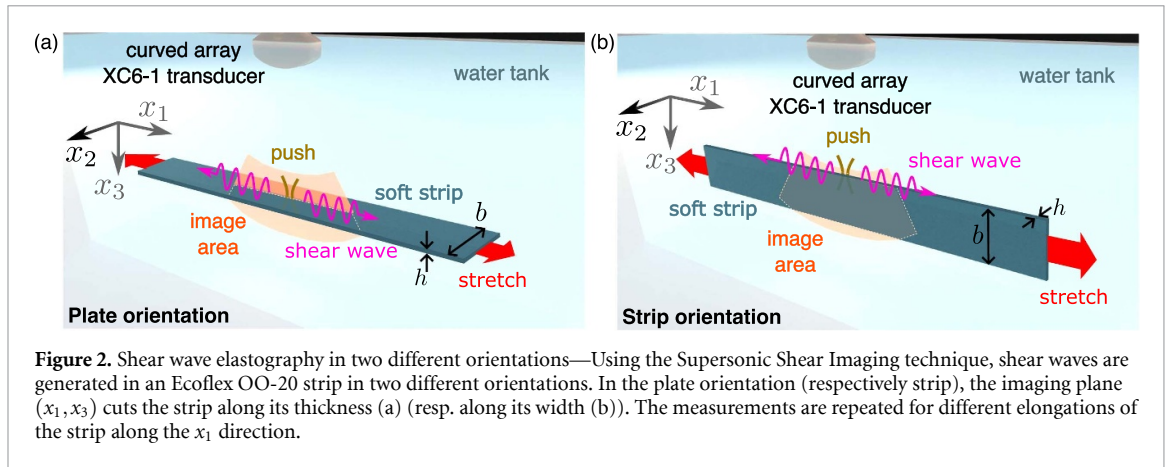


**Figure 2.** Shear wave elastography in two different orientations—Using the Supersonic Shear Imaging technique, shear waves are generated in an Ecoflex OO-20 strip in two different orientations. In the plate orientation (respectively strip), the imaging plane  $(x_1, x_3)$  cuts the strip along its thickness (a) (resp. along its width (b)). The measurements are repeated for different elongations of the strip along the  $x_1$  direction.

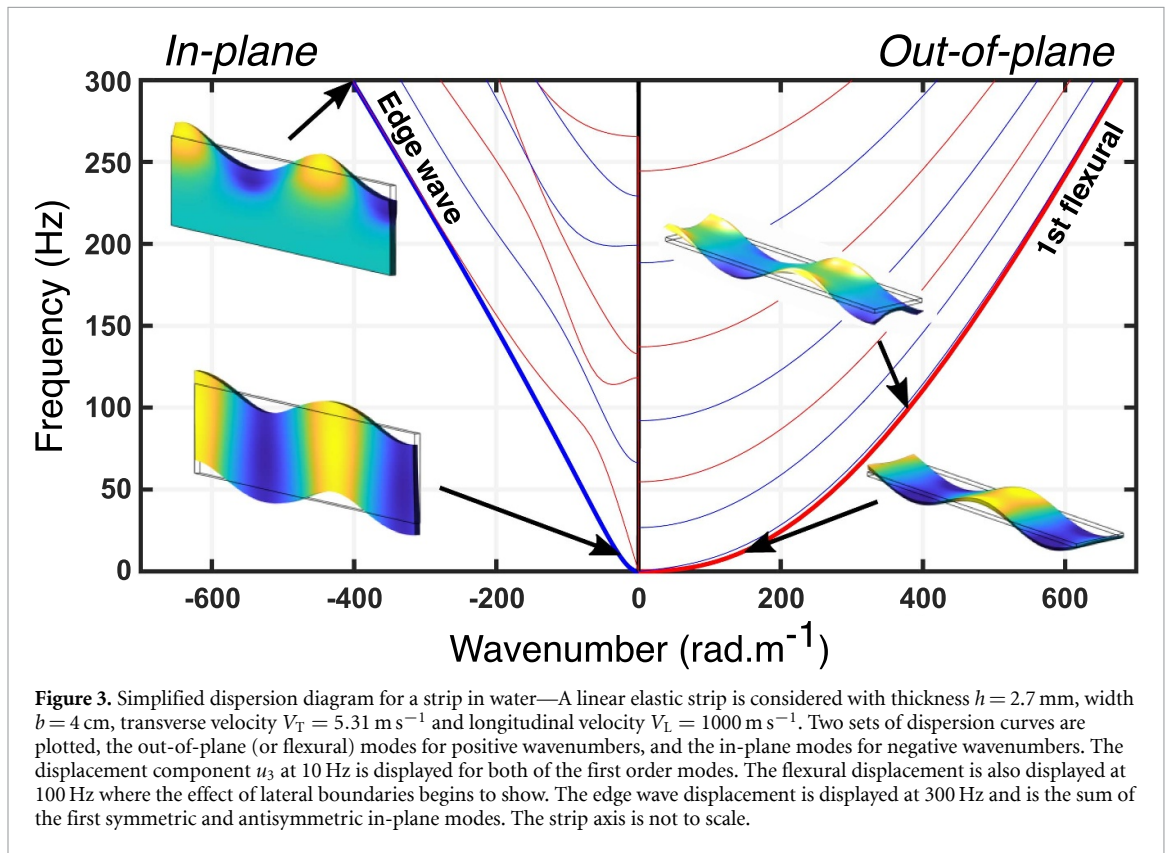


**Figure 3.** Simplified dispersion diagram for a strip in water—A linear elastic strip is considered with thickness  $h = 2.7$  mm, width  $b = 4$  cm, transverse velocity  $V_T = 5.31$  m s<sup>-1</sup> and longitudinal velocity  $V_L = 1000$  m s<sup>-1</sup>. Two sets of dispersion curves are plotted, the out-of-plane (or flexural) modes for positive wavenumbers, and the in-plane modes for negative wavenumbers. The displacement component  $u_3$  at 10 Hz is displayed for both of the first order modes. The flexural displacement is also displayed at 100 Hz where the effect of lateral boundaries begins to show. The edge wave displacement is displayed at 300 Hz and is the sum of the first symmetric and antisymmetric in-plane modes. The strip axis is not to scale.

#### 2.4. Addition of initial pre-stress

To describe waves in a pre-deformed viscoelastic body, one needs first to take into account the behaviour of the medium with respect to initial static pre-stress, then its visco-elastic response to small dynamic deformations.

**Hyperelasticity** — To model the hyperelastic behavior of the strip (Arruda and Boyce 1993, Treloar 2005) subjected to static pre-stress, we assume a compressible Mooney–Rivlin solid. Stretch ratios along all directions  $(\lambda_1, \lambda_2, \lambda_3)$  are introduced, as well as the invariants  $I_1 = \lambda_1^2 + \lambda_2^2 + \lambda_3^2$ ,  $I_2 = \lambda_1^2 \lambda_2^2 + \lambda_1^2 \lambda_3^2 + \lambda_2^2 \lambda_3^2$ , and  $J = \lambda_1 \lambda_2 \lambda_3$ . The strain energy density function  $W$  writes:

$$W = \frac{\mu_0}{2} \left[ (1 - \alpha) \left( \frac{I_1}{J^{2/3}} - 3 \right) + \alpha \left( \frac{I_2}{J^{4/3}} - 3 \right) \right] + \frac{K}{2} (J - 1)^2 \quad (2)$$

where  $\alpha$  governs the behavior of the material ( $\alpha = 0$  corresponds to the Neo-Hookean solid). In the elastography community, it is more common to derive this law in terms of the Landau coefficients  $A$  and  $D$

and an equivalence between the different strategies has already been thoroughly described (Destrade and Ogden 2010, Destrade *et al* 2017).

**Acousto-elasticity** — To describe waves propagating in this pre-deformed viscoelastic body, an incremental approach (Delory *et al* 2023) is constructed as described by Ogden and Destrade (Ogden 1997, Destrade and Saccomandi 2007). The main result of this theory is that the effects of both initial deformation and viscoelasticity can be fully accounted for by introducing a new elastic tensor  $\mathbf{C}^\omega$ . This tensor accounts for the numerous broken symmetries induced by the initial pre-stress, therefore preventing the use of the conventional Cauchy tensor that would describe transverse isotropy for instance. The wave equation writes:

$$\mathbf{C}_{ijkl}^\omega \frac{\partial^2 u'_k}{\partial x_j \partial x_l} + \rho \omega^2 u'_i = 0 \quad (3)$$

with  $\mathbf{u}'(\mathbf{x}, \omega) = \mathbf{x}' - \mathbf{x}$  the incremental monochromatic displacement.  $\mathbf{C}^\omega$  depends on the strain energy density function  $W$ , the stretch ratios  $\lambda_i$ , the rheology of the material and a new material parameter  $\beta'$ . Introducing the specific rheology of equation (1) for the case of Ecoflex-OO20,  $\mathbf{C}^\omega$  decomposes as Delory *et al* (2023):

$$\mathbf{C}_{ijkl}^\omega = \mathbf{C}_{ijkl}^0 + \mu_0 (i\omega\tau)^n \left( 1 + \beta' \frac{\lambda_i^2 + \lambda_j^2 - 2}{2} \right) (\delta_{ik}\delta_{jl} + \delta_{il}\delta_{jk}) \quad (4)$$

where  $\mathbf{C}_{ijkl}^0$  is the equivalent stiffness tensor for the usual acoustoelastic effect (without viscoelasticity) of a hyperelastic solid. Given equation (2) for  $W$ , and knowing the deformation, one can derive the coefficients of the tensor  $\mathbf{C}^0$  with the formulas:

$$C_{iiii}^0 = \frac{\lambda_i \lambda_j}{J} W_{ij} \quad (5)$$

$$C_{ijji}^0 = \frac{\lambda_i^2}{J} \frac{\lambda_i W_i - \lambda_j W_j}{\lambda_i^2 - \lambda_j^2} \quad (i \neq j, \lambda_i \neq \lambda_j) \quad (6)$$

$$C_{ijji}^0 = \frac{C_{iiii}^0 - C_{ijij}^0 + \lambda_i W_i / J}{2} \quad (i \neq j, \lambda_i = \lambda_j) \quad (7)$$

$$C_{ijij}^0 = \frac{\lambda_i \lambda_j}{J} \frac{\lambda_j W_i - \lambda_i W_j}{\lambda_i^2 - \lambda_j^2} \quad (i \neq j, \lambda_i \neq \lambda_j) \quad (8)$$

$$C_{ijij}^0 = \frac{C_{iiii}^0 - C_{ijij}^0 - \lambda_i W_i / J}{2} \quad (i \neq j, \lambda_i = \lambda_j) \quad (9)$$

where  $W_i = \frac{\partial W}{\partial \lambda_i}$  and  $W_{ij} = \frac{\partial^2 W}{\partial \lambda_i \partial \lambda_j}$ . Here, the formulas slightly differ from those found in books (Ogden 1997, Destrade and Saccomandi 2007) because the conventions for dot products are different. To transition from their definition to the one presented in this work, a simple permutation for the last two indices is required. Ultimately, the wave equation to be solved remains the same. It is worth noting that when dealing with intrinsically anisotropic materials, additional invariants should be considered when writing the strain energy density function  $W$  (Balzani *et al* 2006, Peyraut *et al* 2010, Li and Cao 2017, Mukherjee *et al* 2022), but everything can be incorporated in an effective elastic tensor  $\mathbf{C}^\omega$ .

## 2.5. Spectral collocation method to model guided waves in a pre-stressed viscoelastic strip

The newly introduced elastic tensor takes into account both viscoelasticity and initial deformation of the sample. However, this tensor exhibits some broken symmetries that do not conform to the solid mechanics module of COMSOL Multiphysics. To address this issue, we have developed our own calculation code, which is openly accessible (Kiefer *et al* 2023). It implements a semi-analytical technique based on the spectral collocation method (Trefethen 2000, Weideman and Reddy 2000). Semi-analytical methods for guided waves date back to the work by Waas (1972) as well as Kausel and Roësset (1977) for layered media and Aalami (1973) for arbitrary cross-sections. A rather general implementation for plates and cylinders is GEWtool (Kiefer 2023), which is based on spectral elements. The underlying idea of semi-analytical methods is to discretize the cross-section of the waveguide, in our case the thickness and the width of the strip, in order to obtain an eigenvalue problem that can be solved numerically for the waveguide modes. For the present work, we discretize with the spectral collocation method, because it is directly based on the modeled differential equations, and it is accordingly simple to put in place and adapt. For a general overview on

implementing spectral collocation for guided waves in plates (one-dimensional cross-section) refer to Adamou and Craster (2004), Kiefer (2022). Lastly, a concise problem derivation for anisotropic plates is presented in Kiefer *et al* (2023) and for arbitrary cross-sections in Plestenjak *et al* (2024).

For the purpose of this article, the constitutive relation of the stretched viscoelastic elastomer is implemented with the fourth-order stiffness tensor derived from equation (4). After discretization, an equation describing the guided elastic waves with (discrete) displacement field  $u$  on the rectangular cross-section is obtained, namely,

$$\left[ (ik)^2 L_2 + ikL_1 + L_0 + \omega^2 M \right] u = 0, \quad (10)$$

with known matrices  $L_i$  and  $M$ . The above represents an algebraic eigenvalue problem for the eigenpair  $(\omega^2, u)$  parameterized by  $k$ , as is common in commercial softwares such as COMSOL. Alternatively, it can also be solved for the eigenpair  $(k, u)$  parameterized by  $\omega$ , which is particularly useful for frequency-dependent material parameters such as the viscoelastic ones studied here. Choosing different values for  $\omega$  and solving the quadratic eigenvalue problem for  $k$  with conventional methods (e.g. `polyeig` in Matlab) yields the sought dispersion curves  $k(\omega)$ . Note that due to viscoelasticity, the wavenumbers  $k$  are complex-valued, while  $\omega$  remains a real quantity. This is handled naturally by the eigenvalue solver and presents no difficulty.

Although the coupling with the surrounding water is fully incorporated for a plate (Li and Cao 2017, Kiefer *et al* 2019, Gravenkamp *et al* 2025), addressing this issue for a strip goes beyond the scope of the present article. For the sake of simplicity, instead of modelling the leakage in water, we solve the eigenvalue problem for a strip alone and multiply the retrieved wavenumbers by a factor of 1.05, as discussed in appendix.

### 3. Results

We first present the results from the commercial procedure, then we propose a method that could be integrated into existing devices.

#### 3.1. Conventional supersonic shear wave velocities

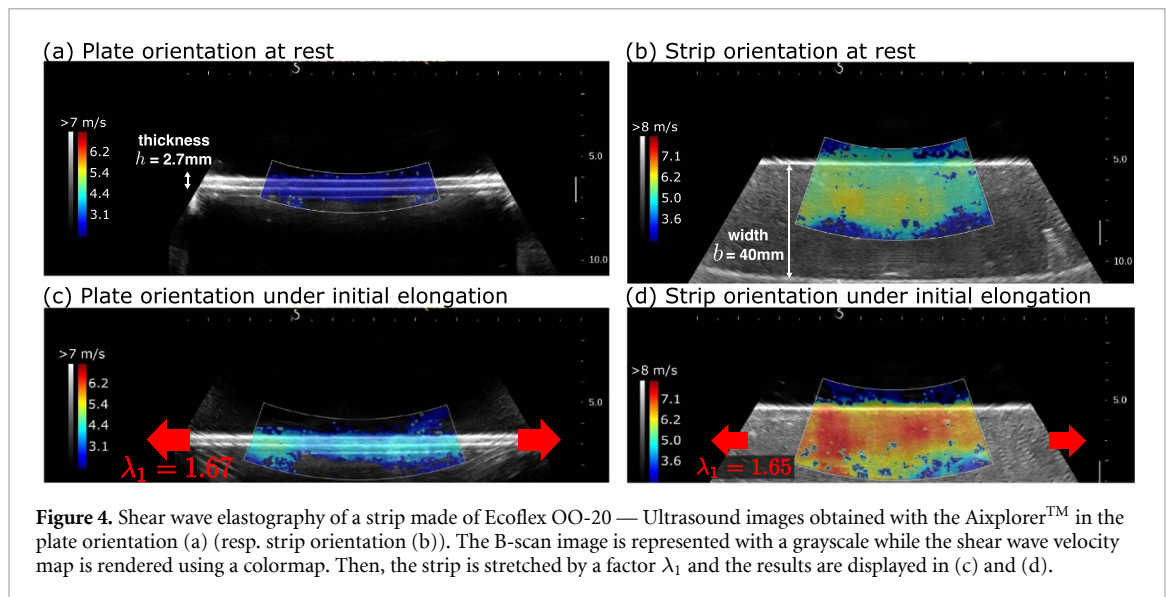
Applying the commercial shear wave elastography procedure described in section 2.2, we probe the shear wave velocity of our Ecoflex strip. We perform the same experiments in both orientations. The measured velocities are displayed as a color code on figures 4(a) and (b) atop the grayscale B-scan images. The measured velocities for the same sample yield significantly different values depending on the orientation considered: in the plate orientation, a velocity of approximately  $3 \text{ m s}^{-1}$  is measured, while in the strip orientation, it is slightly less than  $5 \text{ m s}^{-1}$ . Geometry therefore has an influence on the results.

Additionally, when the same Ecoflex strip is subjected to initial elongation, the measured velocities are also modified, as shown in figures 4(c) and (d). Both of them differ from the velocities measured without initial elongation. They have both increased, reaching  $4 \text{ m s}^{-1}$  for the plate orientation and  $6.5 \text{ m s}^{-1}$  for the strip orientation. Such changes in velocities are attributed to the acousto-elastic effect (Catheline *et al* 2003, Destrade and Saccomandi 2007, Gennisson *et al* 2007, Crutison *et al* 2022).

#### 3.2. Shear wave spectroscopy

In this subsection, we examine the raw data of the shear wave elastography experiment. Instead of extracting a single velocity as shown in figure 4, we perform shear-wave spectroscopy to capture the frequency-dependence of the velocities (Gennisson *et al* 2010, Nguyen *et al* 2011, Deffieux *et al* 2015). The Aixplorer™ in research mode enables the extraction of the full beamformed sequence of images after the release of a push line. The displacement field  $u_3(x_1, x_3, t)$  is obtained by calculating the phase of the correlation between two consecutive images (Bercoff *et al* 2004). Each image sequence is captured five times, and the resulting displacement fields are averaged to improve the signal-to-noise ratio.

The datasets, consisting of 2D movies, need to be reduced for visualization purposes. For the plate orientation, the displacement is supposed to be constant along the thickness (direction  $x_3$ ). Therefore, we decide to average the values along the thickness, resulting in an average spatio-temporal displacement for each push line. The result for the push in the middle of the scanned area is depicted in figure 5(a). For the strip orientation, the post-processing is slightly different because the displacement in the strip varies along



$x_3$ . In fact, only the top strip edge displacement can be studied in an unbiased manner<sup>1</sup>. The spatio-temporal displacement map corresponding to this top edge displacement is shown in figure 5(c).

Applying a spatial and temporal Fourier transform to the reduced displacement map  $u_3(x_1, t)$  provides a frequency versus wavenumber map. The use of a curved-array probe and therefore the imaging of a wider region of the strip allows for a good resolution of the resulting reciprocal space maps. The magnitude of these maps is normalized for each of the five push lines and summed to obtain the graphs shown in figures 5(b) and (d). They are not local data as they represent an average over the entire scanned area. From these graphs, we extract the wavenumber that corresponds to the observed maximum for each frequency, which gives us our dataset.

### 3.3. Systematic extraction of the dispersion curves

The processed experimental results are represented as symbols in figure 6 for all deformed configurations. Frequencies above 300 Hz are discarded due to the lack of signal above this range. We also remove frequencies below 20 Hz for the plate orientation and 90 Hz for the strip orientation due to the signal becoming discontinuous. Phase velocities  $V_\phi = \omega/k$  are extracted from the dispersion curves and the quantity  $\rho V_\phi^2$ , akin to a shear modulus, is plotted as a function of the frequency in figure 6.

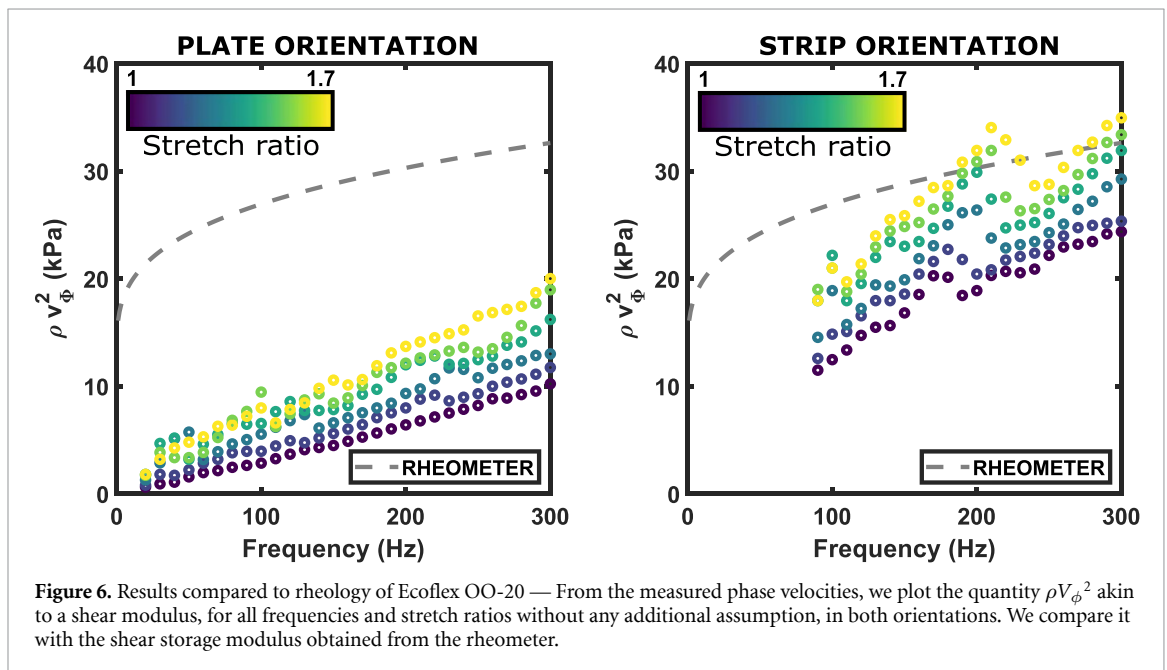
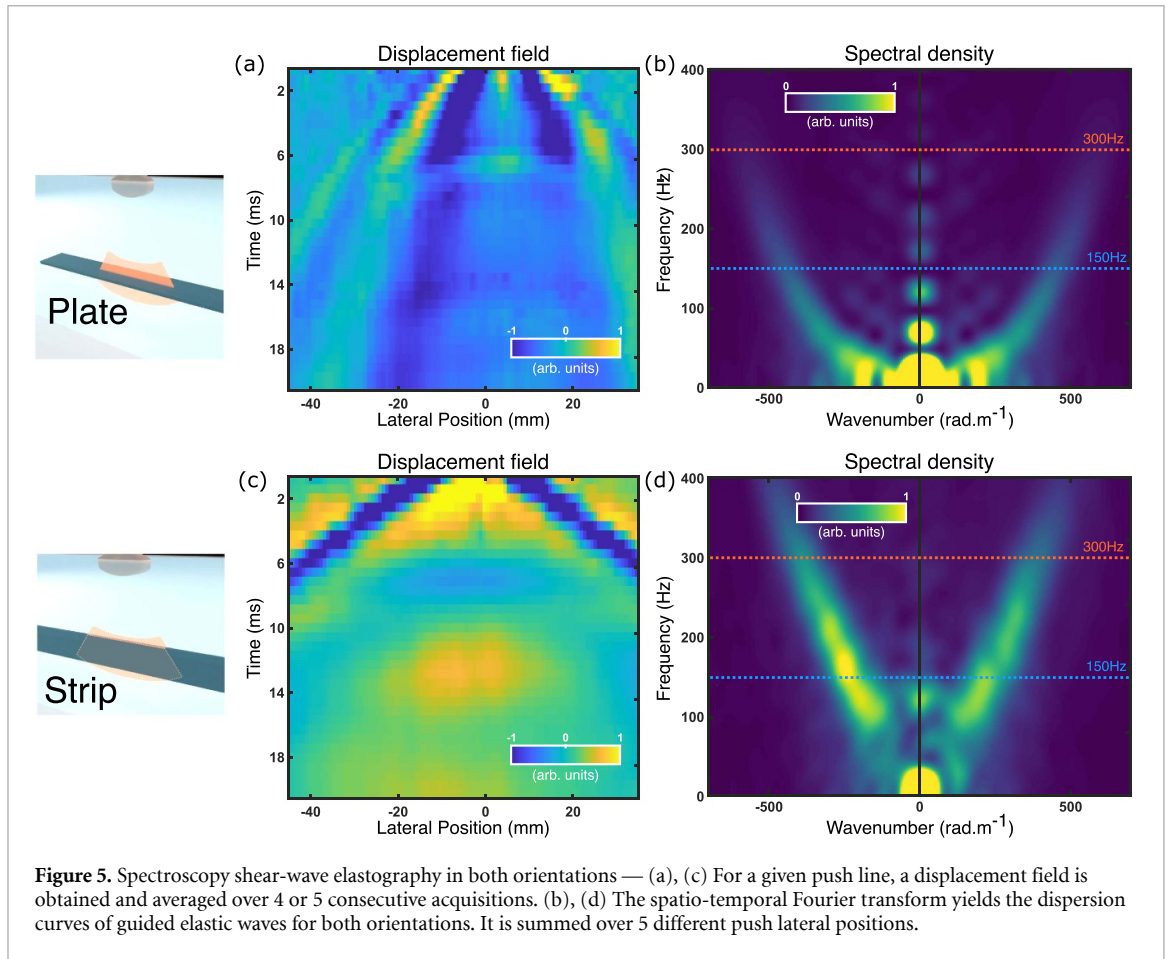
## 4. Discussion

The standard technique used on conventional elastography devices defines the shear modulus and the Young's modulus directly from the shear wave velocity:  $\mu = \rho V_T^2$  and  $E = 3\rho V_T^2$ . Indeed, the elastomer used for our sample is nearly-incompressible, the longitudinal velocity of the propagating waves  $V_L$  is considered constant and all the variability in the measurement comes from  $V_T$ . And, as the contrast between the shear velocity and the longitudinal velocity is large,  $\mu$  and  $E$  are directly calculated from  $V_T^2$ .

With no supplementary assumption on the geometry of the sample, figure 6 reveals an increase in velocity with the frequency and with the stretch ratio. A wide range of values from 1 kPa to 35 kPa is obtained on one unique strip if the shear modulus is directly defined from this velocity according to the conventional method. Moreover, figure 6 shows that none of these values match the data derived from the rheometer in plate-plate configuration (superimposed as a dashed line). These experiments therefore clearly highlight the errors induced by the assumption of bulk shear wave propagation, as already stated and observed in thin biological tissues like arteries (Couade *et al* 2010). More importantly, we provide a comprehensive explanation of this wide range of measured velocities as we discuss in the next parts.

<sup>1</sup> The reason is that the longitudinal velocity used for imaging was assumed to be equal to that of water, which is  $1480 \text{ m s}^{-1}$ , but sound propagates at around  $1000 \text{ m s}^{-1}$  in our material. This implies two additional difficulties. Firstly, the  $x_3 = ct$  axis is properly computed between the transducer and the top strip edge, but in the strip, this axis is wrongly estimated, and the beamforming procedure is biased. This is visible in figure 4(b), where the bottom edge appears curved in the B-mode image. Secondly, the push focusing must also be degraded when going deeper into the strip.

<sup>2</sup> Our sample has no intrinsic anisotropy that would induce variability of  $V_T$  depending on the direction of wave propagation.



#### 4.1. Identification of the guided modes

Let us begin by highlighting the guiding property that underlies the different velocities observed for the plate orientation and the strip orientation (figures 4–6). On the raw data of figure 5, we can observe that the displacement at the central position at time  $t = 0$  (top line) symmetrically propagates as time increases (echoes emerging at the abscissa of the push, at respectively 8 ms and 13 ms for the plate and strip orientations, must not be mixed up with the generated waves). However, the behavior depends on the orientation: in the strip orientation, the shear wave reaches the edges of the scanned area sooner than in the

plate one. Additionally, the propagation exhibits a linear shape for the strip orientation, while the wavefronts are bent in the plate orientation: short wavelengths travel faster than long ones, revealing dispersive propagation.

The differences between the two orientations are clearly highlighted by the corresponding frequency versus wavenumber maps in figures 5(b) and (d). A quadratic-shaped dispersion relation is observed for the plate orientation, while a linear dispersion relation is observed for the strip orientation. Additionally, intensity of the displacement depends on the frequency. In the plate orientation, intensities are high in the low-frequency range and fade rapidly as frequency increases, almost disappearing around 300 Hz. On the contrary, energy is found at higher frequencies in the strip orientation, with maximal intensity around 150 Hz (excluding the zero-frequency spot). Lastly, we notice some spots for certain frequencies on the  $k = 0$  axis in both orientations. These spots are due to echoes of waves reflecting on the edges of the strip. In a waveguide, these reverberations usually materialize as cut-off frequencies in the dispersion diagram.

The comparison of these dispersion relations with the simulation of guided waves in a strip immersed in water (figure 3) is relatively straightforward because the dispersion curves are well separated, compared to arteries for instance where modes of similar shapes are generated (Astaneh *et al* 2017) and where mixing between flexural modes (Roy *et al* 2021) can be observed. In the plate orientation, the radiation force-induced push corresponds to an out-of-plane displacement of the strip, and the generated guided wave is therefore the first flexural out-of-plane mode displayed in figure 3 with a thick red line. Its power-law behavior is a well-known characteristic of a bending mode (Delory *et al* 2024). Alternatively, for the strip orientation, the pushes generate an in-plane displacement in the strip, corresponding to the first antisymmetrical mode (or a combination of the first antisymmetrical mode and the first symmetrical mode for higher frequencies). Its dispersion curve is plotted as a thick blue line with negative wavenumbers in figure 3. Again, the displacement profile of this mode at 10 Hz and 300 Hz is compatible with an excitation at the top edge of the strip. At 10 Hz, this mode is, in fact, dispersive since it is very similar to a bending of the strip, but this time in its width. When increasing the frequency, the wavelength decreases, and the width of the guide becomes larger than the shear wavelength: most of the mode's energy is now confined to the edge of the strip.

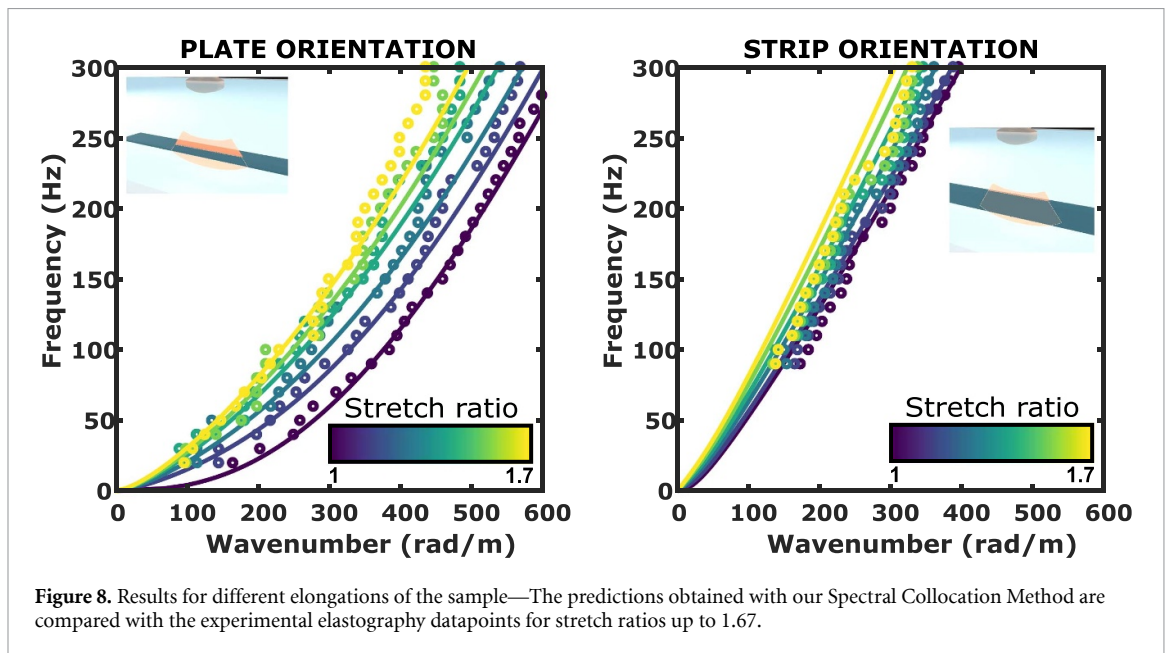
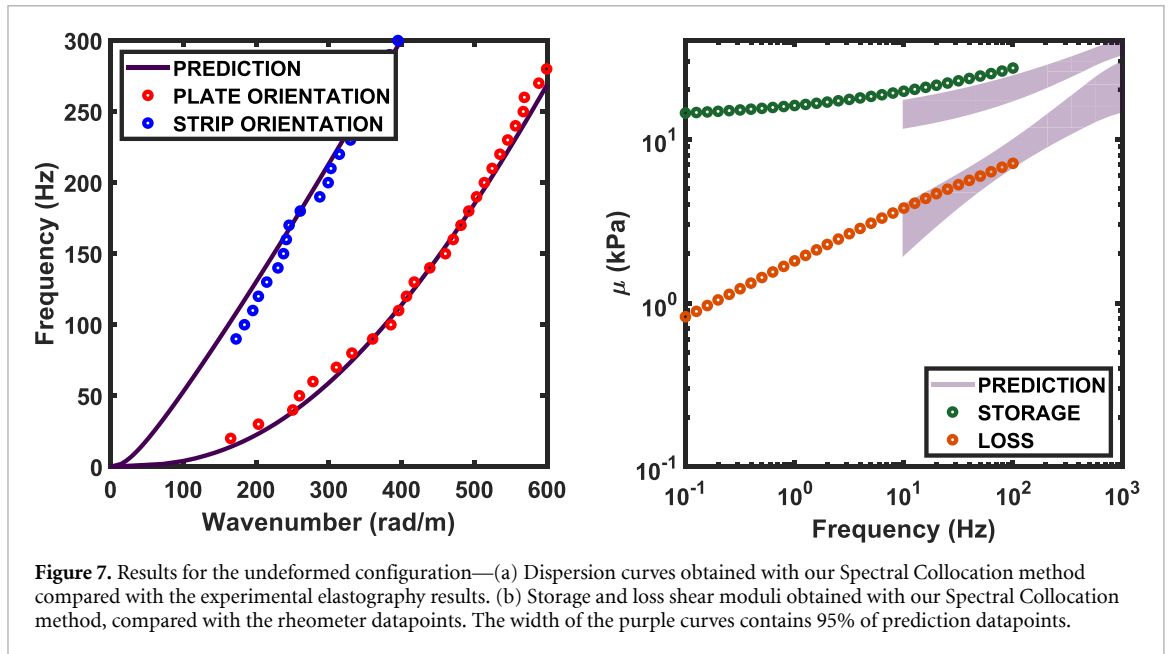
#### 4.2. Spectral collocation method to account for viscoelasticity and initial deformation

In a non-viscous case, the edge mode generated in the strip orientation is theoretically almost non-dispersive. However, the experimental phase velocity  $V_\phi$  of this mode, given by the dispersion curves in figure 5, is equal to  $4 \text{ m s}^{-1}$  at 150 Hz and  $4.8 \text{ m s}^{-1}$  at 300 Hz. This dispersion is due to the viscoelasticity of the medium i.e. its frequency-dependent material properties, described by equation (1). Similar dispersion has already been observed in gel phantoms and muscle tissues (Catheline *et al* 2004, Chen *et al* 2004).

The spectral collocation method fully incorporates the rheology of the material and the guiding geometry (see section 2.5). Resulting theoretical predictions for a strip of Ecoflex OO-20 of thickness  $h = 2.7 \text{ mm}$  and width  $b = 4 \text{ cm}$  are superimposed as solid lines on the experimental data of figure 7. The rheological parameters  $\mu_0 = 11 \text{ kPa}$ ,  $\tau = 2.3 \text{ ms}$ , and  $n = 0.44$  were obtained after a minimisation procedure to fit the prediction to the experimental dispersion curves. Here,  $n \neq 1$  validates the fractional-derivative model, necessitating a supplementary parameter compared to the classical Voigt model (Roy and Guddati 2023). Figure 7(a) displays a very good agreement between the datapoints from our elastography experiments and the dispersion curves corresponding to these parameters. Additionally, in figure 7(b), we extend the conventional rheometer measurements from figure 1 with the shear modulus calculated using our method and the above parameters (see section 2.1), on the frequency range of our elastography measurements. Statistics were performed on the different shear moduli obtained by iteration of our minimisation procedure to quantify its accuracy. Our estimated shear moduli are a good higher-frequency extension of the rheometer datapoints. The small gap between the shear storage moduli could be due to differences in polymerization in the rheometer and in our experimental strip, happening on a scale smaller than 1 mm for the former and around 1 cm for the latter.

Additionally, the ultrasound scanner allows us to measure shear wave propagation for several values of  $\lambda_1$  ranging from 1 (undeformed) to 1.67. For each stretch ratio and both orientations, the dispersion relations are extracted. Figure 8 compares them with theoretical dispersion curves obtained using our spectral collocation framework (see section 2.5). Acoustoelasticity explains the shift of the dispersion curves caused by the increase of the stretch ratio (see section 2.4): in addition to the optimized rheological parameters listed in the above paragraph,  $\alpha = 0.27$  and  $\beta' = 0.43$  are the optimized acoustoelastic parameters.

In both orientations, applying a static stress tends to increase the slopes of the dispersion curves: the higher the stretching, the higher the frequency for a given wavenumber. Put differently, the velocity of the



wave guided along the stretched direction is increased. This is a relatively intuitive behavior that can be easily experienced with a tensed string. However, while the general trend is easy enough to conceptualize, the details of the increase are harder to grasp.

The stretch-induced velocity change, called the acoustoelastic effect, is particularly significant in biological tissues (Holzapfel and Ogden 2010, Chagnon *et al* 2015) and more generally in soft media, which are highly deformable. It has already been studied in elastography for uniaxial (Salehabadi *et al* 2023) or planar (Dore *et al* 2022) strains but the consideration of viscoelasticity is lacking. An experimental study on Ecoflex with MRE (Brinker and Klatt 2016) also reveals changes of shear modulus with elongation ratio but the mechanical model remains simple. Here, we would like to emphasize that the theoretical framework recalled in sections 2.4 and 2.5, relying first on the modeling of a large static deformation and then considering the propagation of small perturbations, is perfectly suited to explain these results. This approach has already been investigated in a similar elastomer with guided waves in a plate (Delory *et al* 2023) and in a strip (Delory *et al* 2024). It was shown that hyperelastic and viscoelastic material properties must be taken into account simultaneously.

For the plate orientation, the predictions provided by our approach in figure 8 are very satisfactory for stretch ratios up to 1.5. For the strip orientation, the predictions overestimate slightly the phase velocities but are still very satisfactory for all stretch ratios. The remaining errors may be due to the oversimplified model that has been used (see appendix). Secondly, errors can also be attributed to the non-linear material model: the involved hyperelastic model (Mooney–Rivlin, see section 2.4) remains a weakly nonlinear elastic model.

Based on these interesting results, we can imagine the implementation of an inverse method to simultaneously evaluate the rheological and the hyperelastic parameters. Alternatively, as the geometric parameters ( $h, b$ ) of the sample also have an influence on the shape of the dispersion curves, especially on cut-off frequencies, ultrasound images could be used to monitor their evolution with the applied prestress.

## 5. Conclusion

The influence of guiding geometry, frequency, and static deformation in elastography is addressed in this study, utilizing a single material, straightforward experimental method and robust modeling. We demonstrate that overlooking these factors may yield a broad spectrum of inaccurate shear moduli. The methodology outlined here can be readily adapted to accommodate various material models, including anisotropic ones, and may be extended to encompass diverse guiding geometries.

Furthermore, our approach suggests the potential for solving the inverse problem, allowing the inference of hyperelastic and viscoelastic properties from measured dispersion curves on a soft material.

We contend that the simultaneous effect of elongation, guiding geometry and viscoelasticity can encapsulate numerous physiological scenarios: from the stretching of muscles and tendons to the propagation of pulsatile waves in arteries (Baranger *et al* 2023), or even the compression of tissues during ultrasound examination. The availability of a versatile tool such as the Spectral Collocation Method, adept at integrating these multifaceted aspects, holds promise for enhancing the quantitiveness of elastography and fortifying its foundations within robust clinical databases.

## Data availability statement

All data that support the findings of this study are included within the article (and any supplementary information files).

## Acknowledgment

We would like to acknowledge the valuable help of Arthur Le Ber and Flavien Bureau for the use of the Aixplorer<sup>TM</sup> ultrasound system. This work has received support under the program ‘Investissements d’Avenir’ launched by the French Government and was partially supported by the Simons Foundation/Collaboration on Symmetry-Driven Extreme Wave Phenomena. A D acknowledges funding from French Direction Générale de l’Armement.

## Appendix. Role of water on the dispersion relations

Using COMSOL Multiphysics, it is possible to compare the dispersion diagrams of a soft strip in air or immersed in water (figure A1) as in the described experiments. The coupling with water has a significant effect on flexural modes, that displace an additional quantity of water, thus adding inertia and lowering the dispersion curves. On the other hand, the effect is weaker on the in-plane guided modes.

Additionally, the dispersion curve of the first flexural mode of a plate is included (black solid line in figure A1). One notices that it almost coincides with the first flexural mode that propagates in the strip. This observation is important because it allows comparison with theoretical predictions for a plate immersed in water (Sun *et al* 2022).

For the in-plane mode of interest, it seems that the velocity is decreased by 5% when the coupling with water is added. Consequently, we multiply the wavenumbers by 1.05 to simulate the influence of water when calculating solutions in its absence with the Spectral Collocation Code.

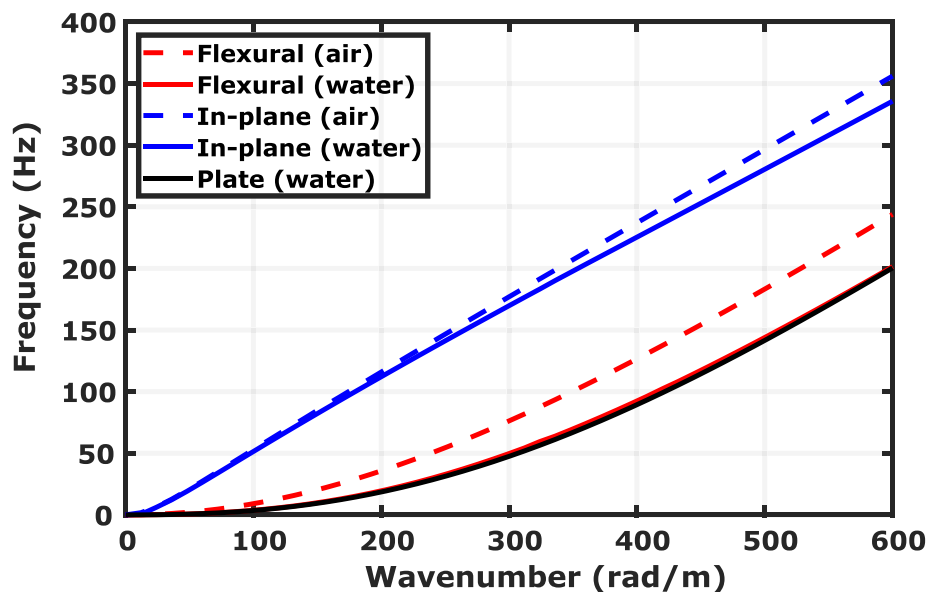


**Figure A1.** Dispersion curves of the two modes of interest for a strip in air and water—A purely elastic strip is considered with a thickness  $h = 2.7$  mm, a width  $b = 4$  cm and a transverse velocity  $V_T = 4 \text{ m s}^{-1}$ . The out-of-plane (or flexural) mode is mainly polarized along the thickness axis while the in-plane mode is mainly polarized in the plane of the width and propagation axis. Two dispersion diagrams are superimposed: with (full lines) and without (dashed lines) coupling with water.

## References

- Aalami B 1973 Waves in prismatic guides of arbitrary cross section *J. Appl. Mech.* **40** 1067–72
- Adamou A T I and Craster R V 2004 Spectral methods for modelling guided waves in elastic media *J. Acoust. Soc. Am.* **116** 1524–35
- Arruda E M and Boyce M C 1993 A three-dimensional constitutive model for the large stretch behavior of rubber elastic materials *J. Mech. Phys. Solids* **41** 389–412
- Asbach P et al 2010 Viscoelasticity-based Staging of Hepatic Fibrosis with Multifrequency MR Elastography *Radiology* **257** 80–86
- Astaneh A V, Urban M W, Aquino W, Greenleaf J F and Guddati M N 2017 Arterial waveguide model for shear wave elastography: implementation and in vitro validation *Phys. Med. Biol.* **62** 5473
- Bagley R L and Torvik P J 1983 Fractional calculus—a different approach to the analysis of viscoelastically damped structures *AIAA J.* **21** 741–8
- Balzani D, Neff P, Schröder J and Holzapfel G A 2006 A polyconvex framework for soft biological tissues. Adjustment to experimental data *Int. J. Solids Struct.* **43** 6052–70
- Baranger J, Villemain O, Goudot G, Dizeux A, Blay H L, Mirault T, Messas E, Pernot M and Tanter M 2023 The fundamental mechanisms of the korotkoff sounds generation *Sci. Adv.* **9** eadi4252
- Barr R G 2019 Future of breast elastography *Ultrasonography* **38** 93–105
- Barr R G and Zhang Z 2012 Effects of precompression on elasticity imaging of the breast *J. Ultrasound Med.* **31** 895–902
- Bercoff J, Tanter M and Fink M 2004 Supersonic shear imaging: a new technique for soft tissue elasticity mapping *IEEE Trans. Ultrason. Ferroelectr. Freq. Control* **51** 396–409
- Bilston L E 2018 Soft tissue rheology and its implications for elastography: challenges and opportunities *NMR Biomed.* **31** e3832
- Brinker S and Klatt D 2016 Demonstration of concurrent tensile testing and magnetic resonance elastography *J. Mech. Behav. Biomed. Mater.* **63** 232–43
- Caenen A, Pernot M, Nightingale K R, Voigt J-U, Vos H J, Segers P and D’hooge J 2022 Assessing cardiac stiffness using ultrasound shear wave elastography *Phys. Med. Biol.* **67** 02TR01
- Cantisani V et al 2015 Strain US elastography for the characterization of thyroid nodules: advantages and limitation *Int. J. Endocrinol.* **2015** e908575
- Catheline S, Gennisson J-L, Delon G, Fink M, Sinkus R, Abouelkaram S and Culioli J 2004 Measurement of viscoelastic properties of homogeneous soft solid using transient elastography: an inverse problem approach *J. Acoust. Soc. Am.* **116** 3734–41
- Catheline S, Gennisson J-L and Fink M 2003 Measurement of elastic nonlinearity of soft solid with transient elastography *J. Acoust. Soc. Am.* **114** 3087–91
- Chagnon G, Rebouah M and Favier D 2015 Hyperelastic energy densities for soft biological tissues: a review *J. Elast.* **120** 129–60
- Chen S, Fatemi M and Greenleaf J F 2004 Quantifying elasticity and viscosity from measurement of shear wave speed dispersion *J. Acoust. Soc. Am.* **115** 2781–5
- Correas J-M, Tissier A-M, Khairoune A, Khoury G, Eiss D and Hélénon O 2013 Ultrasound elastography of the prostate: state of the art *Diag. Intervent. Imaging* **94** 551–60
- Couade M, Pernot M, Prada C, Messas E, Emmerich J, Bruneval P, Criton A, Fink M and Tanter M 2010 Quantitative assessment of arterial wall biomechanical properties using shear wave imaging *Ultrasonography Med. Biol.* **36** 1662–76
- Crutison J, Sun M and Royston T J 2022 The combined importance of finite dimensions, anisotropy and pre-stress in acoustoelastography *J. Acoust. Soc. Am.* **151** 2403–13
- Davis L C, Baumer T G, Bey M J and van Holsbeeck M V 2019 Clinical utilization of shear wave elastography in the musculoskeletal system *Ultrasonography* **38** 2–12
- Deffieux T 2008 Palpation par force de radiation ultrasonore et échographie ultrarapide: applications à la caractérisation tissulaire *in vivo Thèse de doctorat Université Paris 7 - Paris Diderot, Institut Langevin*

- Deffieux T et al 2015 Investigating liver stiffness and viscosity for fibrosis, steatosis and activity staging using shear wave elastography *J. Hepatol.* **62** 317–24
- Delory A, Kiefer D A, Lanoy M, Eddi A, Prada C and Lemoult F 2024 Viscoelastic dynamics of a soft strip subject to a large deformation *Soft Matter* **20** 1983–95
- Delory A, Lemoult F, Eddi A and Prada C 2023 Guided elastic waves in a highly-stretched soft plate *Extreme Mech. Lett.* **61** 102018
- Delory A, Lemoult F, Lanoy M, Eddi A and Prada C 2022 Soft elastomers: a playground for guided waves *J. Acoust. Soc. Am.* **151** 3343–58
- Destrade M and Ogden R W 2010 On the third- and fourth-order constants of incompressible isotropic elasticity *J. Acoust. Soc. Am.* **128** 3334–43
- Destrade M and Saccomandi G 2007 *Waves in Nonlinear pre-Stressed Materials (Number 495 in Cism Courses and Lectures)* (Springer)
- Destrade M, Saccomandi G and Sgura I 2017 Methodical fitting for mathematical models of rubber-like materials *Proc. R. Soc. A* **473** 20160811
- Doherty J R, Trahey G E, Nightingale K R and Palmeri M L 2013 Acoustic radiation force elasticity imaging in diagnostic ultrasound *IEEE Trans. Ultrason. Ferroelectr. Freq. Control* **60** 685–701
- Dore M, Luna A and Royston T J 2022 Biaxial tensile prestress and waveguide effects on estimates of the complex shear modulus using optical-based dynamic elastography in plate-like soft tissue phantoms *J. Eng. Sci. Med. Diag. Therapy* **6** 011006
- Elgeti T and Sack I 2014 Magnetic resonance elastography of the heart *Curr. Cardiovascular Imaging Rep.* **7** 9247
- Farron J, Varghese T and Thelen D G 2009 Measurement of tendon strain during muscle twitch contractions using ultrasound elastography *IEEE Trans. Ultrason. Ferroelectr. Freq. Control* **56** 27–35
- Gennisson J-L, Deffieux T, Macé E, Montaldo G, Fink M and Tanter M 2010 Viscoelastic and anisotropic mechanical properties of *in vivo* muscle tissue assessed by supersonic shear imaging *Ultrasound Med. Biol.* **36** 789–801
- Gennisson J-L, Rénier M, Catheline S, Barrière C, Bercoff J, Tanter M and Fink M 2007 Acoustoelasticity in soft solids: assessment of the nonlinear shear modulus with the acoustic radiation force *J. Acoust. Soc. Am.* **122** 3211–9
- Gravenkamp H, Plestenjak B, Kiefer D A and Jarlebring E 2025 Computation of leaky waves in layered structures coupled to unbounded media by exploiting multiparameter eigenvalue problems *J. Sound Vib.* **596** 118716
- Hansen H H G, Pernot M, Chatelin S, Tanter M and de Korte C L 2015 Shear wave elastography for lipid content detection in transverse arterial cross-sections *2015 IEEE Int. Ultrasonics Symp. (IUS)* pp 1–4
- Henni A H, Schmitt C, Tremblay M-E, Hamdine M, Heuzey M-C, Carreau P and Cloutier G 2011 Hyper-frequency viscoelastic spectroscopy of biomaterials *J. Mech. Behav. Biomed. Mater.* **4** 1115–22
- Hiscox L V, Johnson C L, Barnhill E, McGarry M D J, Huston J, van Beek E J R, Starr J M and Roberts N 2016 Magnetic resonance elastography (MRE) of the human brain: technique, findings and clinical applications *Phys. Med. Biol.* **61** R401
- Holzapfel G A and Ogden R W 2010 Constitutive modelling of arteries *Proc. R. Soc. A* **466** 1551–97
- Kausel E and Roësset J M 1977 Semianalytic hyperelement for layered strata *J. Eng. Mech. Div.* **103** 569–88
- Kearney S P, Khan A, Dai Z and Royston T J 2015 Dynamic viscoelastic models of human skin using optical elastography *Phys. Med. Biol.* **60** 6975
- Kennedy B F, Kennedy K M and Sampson D D 2014 A review of optical coherence elastography: fundamentals, techniques and prospects *IEEE J. Sel. Top. Quantum Electron.* **20** 272–88
- Kennedy P, Wagner M, Castéra L, Hong C W, Johnson C L, Sirlin C B and Taouli B 2018 Quantitative elastography methods in liver disease: current evidence and future directions *Radiology* **286** 738–63
- Khan S, Fakhouri F, Majeed W and Kolipaka A 2018 Cardiovascular magnetic resonance elastography: a review *NMR Biomed.* **31** e3853
- Kiefer D A 2022 *Elastodynamic Quasi-Guided Waves for Transit-Time Ultrasonic Flow Metering (FAU Forschungen, Reihe B, Medizin, Naturwissenschaft, Technik)* (FAU University Press)
- Kiefer D A 2023 Gewtool (<https://doi.org/10.5281/zenodo.10114243>)
- Kiefer D A, Delory A and Lemoult F 2023 GEW soft strip (<https://doi.org/10.5281/zenodo.10641373>)
- Kiefer D A, Plestenjak B, Gravenkamp H and Prada C 2023 Computing zero-group-velocity points in anisotropic elastic waveguides: globally and locally convergent methods *J. Acoust. Soc. Am.* **153** 1386–98
- Kiefer D A, Ponschab M, Rupitsch S J and Mayle M 2019 Calculating the full leaky Lamb wave spectrum with exact fluid interaction *J. Acoust. Soc. Am.* **145** 3341–50
- Kirby M A, Pelivanov I, Song S, Ambrozinski L, Yoon S J, Gao L, Li D, Shen T T, Wang R K and O'Donnell M 2017 Optical coherence elastography in ophthalmology *J. Biomed. Opt.* **22** 121720
- Lan G, Twa M D, Song C, Feng J, Huang Y, Xu J, Qin J, An L and Wei X 2023 *In vivo* corneal elastography: a topical review of challenges and opportunities *Comput. Struct. Biotechnol. J.* **21** 2664–87
- Lanoy M, Lemoult F, Eddi A and Prada C 2020 Dirac cones and chiral selection of elastic waves in a soft strip *Proc. Natl Acad. Sci.* **117** 30186–90
- Leartprapun N and Adie S G 2023 Recent advances in optical elastography and emerging opportunities in the basic sciences and translational medicine [Invited] *Biomed. Opt. Express* **14** 208–48
- Li G-Y and Cao Y 2017 Mechanics of ultrasound elastography *Proc. R. Soc. A* **473** 20160841
- Li G-Y, He Q, Mangan R, Xu G, Mo C, Luo J, Destrade M and Cao Y 2017 Guided waves in pre-stressed hyperelastic plates and tubes: application to the ultrasound elastography of thin-walled soft materials *J. Mech. Phys. Solids* **102** 67–79
- Liao Z, Yang J, Hossain M, Chagnon G, Jing L and Yao X 2021 On the stress recovery behaviour of Ecoflex silicone rubbers *Int. J. Mech. Sci.* **206** 106624
- Liu Y, Yasar T K and Royston T J 2014 Ultra wideband (0.5–16 kHz) MR elastography for robust shear viscoelasticity model identification *Phys. Med. Biol.* **59** 7717
- Low G, Kruse S A and Lomas D J 2016 General review of magnetic resonance elastography *World J. Radiol.* **8** 59–72
- Mainardi F 2022 *Fractional Calculus and Waves in Linear Viscoelasticity: an Introduction to Mathematical Models* (World Scientific)
- Marlevi D et al 2020 Combined spatiotemporal and frequency-dependent shear wave elastography enables detection of vulnerable carotid plaques as validated by MRI *Sci. Rep.* **10** 403
- Mifsud T, Gatt A, Micallef-Stafrace K, Chockalingam N and Padhiar N 2023 Elastography in the assessment of the Achilles tendon: a systematic review of measurement properties *J. Foot Ankle Res.* **16** 23
- Mukherjee S, Destrade M and Gower A L 2022 Representing the stress and strain energy of elastic solids with initial stress and transverse texture anisotropy *Proc. R. Soc. A* **478** 20220255

- Nguyen T-M, Couade M, Bercoff J and Tanter M 2011 Assessment of viscous and elastic properties of sub-wavelength layered soft tissues using shear wave spectroscopy: Theoretical framework and in vitro experimental validation *IEEE Trans. Ultrason. Ferroelectr. Freq. Control* **58** 2305–15
- Ogden R W 1997 *Non-Linear Elastic Deformations* (Dover Publications)
- Ormachea J and Parker K J 2020 Elastography imaging: the 30 year perspective *Phys. Med. Biol.* **65** 24TR06
- Paluch Lukasz, Nawrocka-Laskus E, Wieczorek J, Mruk B, Frel M and Walecki J 2016 Use of ultrasound elastography in the assessment of the musculoskeletal system *Pol. J. Radiol.* **81** 240–6
- Parker K J, Szabo T and Holm S 2019 Towards a consensus on rheological models for elastography in soft tissues *Phys. Med. Biol.* **64** 215012
- Pelivanov I, Gao L, Pitre J, Kirby M A, Song S, Li D, Shen T T, Wang R K and O'Donnell M 2019 Does group velocity always reflect elastic modulus in shear wave elastography? *J. Biomed. Opt.* **24** 076003
- Peyraut F, Feng Z-Q, Labeled N and Renaud C 2010 A closed form solution for the uniaxial tension test of biological soft tissues *Int. J. Non-Linear Mech.* **45** 535–41
- Plestenjak B, Kiefer D A and Gravenkamp H 2024 A Sylvester equation approach for the computation of zero-group-velocity points in waveguides (<https://doi.org/10.1007/s00466-025-02656-8>)
- Prado-Costa R, Rebelo J ao, Monteiro-Barroso J ao and Preto A S 2018 Ultrasound elastography: compression elastography and shear-wave elastography in the assessment of tendon injury *Insights Imaging* **9** 791–814
- Pruijssen J T, de Korte C L, Voss I and Hansen H H G 2020 Vascular shear wave elastography in atherosclerotic arteries: a systematic review *Ultrasound Med. Biol.* **46** 2145–63
- Ramier A, Tavakol B and Yun S-H 2019 Measuring mechanical wave speed, dispersion and viscoelastic modulus of the cornea using optical coherence elastography *Opt. Express* **27** 16635
- Rolley E, Snoeijer J H and Andreotti B 2019 A flexible rheometer design to measure the visco-elastic response of soft solids over a wide range of frequency *Rev. Sci. Instrum.* **90** 023906
- Roy T and Guddati M N 2023 Full waveform inversion for arterial viscoelasticity *Phys. Med. Biol.* **68** 05NT02
- Roy T, Urban M, Xu Y, Greenleaf J and Guddati M N 2021 Multimodal guided wave inversion for arterial stiffness: methodology and validation in phantoms *Phys. Med. Biol.* **66** 115020
- Sack I 2023 Magnetic resonance elastography from fundamental soft-tissue mechanics to diagnostic imaging *Nat. Rev. Phys.* **5** 25–42
- Salehabadi M, Nammari L, Luna A, Crutison J, Klatt D and Royston T J 2023 Quantifying uniaxial prestress and waveguide effects on dynamic elastography estimates for a cylindrical rod *J. Acoust. Soc. Am.* **154** 3580–94
- Sandrin L et al 2003 Transient elastography: a new noninvasive method for assessment of hepatic fibrosis *Ultrasound Med. Biol.* **29** 1705–13
- Sharma A, Marapureddy S G, Paul A, Bishr S R, Kakkar M, Thareja P and Mercado-Shekhkar K P 2023 Characterizing viscoelastic polyvinyl alcohol phantoms for ultrasound elastography *Ultrasound Med. Biol.* **49** 497–511
- Shiina T 2014 Ultrasound elastography: Development of novel technologies and standardization *Jpn. J. Appl. Phys.* **53** 07KA02
- Sigrist R M S, Liau J, Kaffas A E, Chammass M C and Willmann J K 2017 Ultrasound elastography: review of techniques and clinical applications *Theranostics* **7** 1303–29
- Sinkus R 2014 Elasticity of the heart, problems and potentials *Curr. Cardiovascular Imaging Rep.* **7** 9288
- Sinkus R, Tanter M, Xydeas T, Catheline S, Bercoff J and Fink M 2005 Viscoelastic shear properties of *in vivo* breast lesions measured by MR elastography *Magn. Reson. Imaging* **23** 159–65
- Smit W and De Vries H 1970 Rheological models containing fractional derivatives *Rheol. Acta* **9** 525–34
- Sun M G, Son T, Crutison J, Guaiquil V, Lin S, Nammari L, Klatt D, Yao X, Rosenblatt M I and Royston T J 2022 Optical coherence elastography for assessing the influence of intraocular pressure on elastic wave dispersion in the cornea *J. Mech. Behav. Biomed. Mater.* **128** 105100
- Taljanovic M S, Gimber L H, Becker G W, Latt L D, Klausner A S, Melville D M, Gao L and Witte R S 2017 Shear-wave elastography: basic physics and musculoskeletal applications *RadioGraphics* **37** 855–70
- Trefethen L N 2000 *Spectral Methods in Matlab* (Society for Industrial and Applied Mathematics)
- Treloar L R G 2005 *The Physics of Rubber Elasticity (Oxford Classic Texts in the Physical Sciences)* 3rd edn (Oxford University Press)
- Waas G 1972 Linear two dimensional analysis of soil dynamics problems in semi-infinite layered media *PhD Thesis* University of California
- Weideman J A and Reddy S C 2000 A MATLAB differentiation matrix suite *ACM Trans. Math. Softw.* **26** 465–519
- Winn N, Lalam R and Cassar-Pullicino V 2016 Sonoelastography in the musculoskeletal system: current role and future directions *World J. Radiol.* **8** 868–79
- Yasar T K, Royston T J and Magin R L 2013 Wideband MR elastography for viscoelasticity model identification *Magn. Reson. Med.* **70** 479–89
- Zvietcovich F and Kirill V L 2022 Wave-based optical coherence elastography: the 10-year perspective *Prog. Biomed. Eng.* **4** 012007